MAY 05 2003

Diffraction of sound from a dipole source near to a barrier or an impedance discontinuity

Marc Buret; Kai Ming Li; Keith Attenborough

J. Acoust. Soc. Am. 113, 2480–2494 (2003)
https://doi.org/10.1121/1.1566977

Diffraction of sound from a dipole source near to a barrier or an impedance discontinuity

Marc Buret[a] and Kai Ming Li[b]
Department of Mechanical Engineering, The Hong Kong Polytechnic University, Hong Kong

Keith Attenborough
Department of Engineering, The University of Hull, Hull HU6 7RX, United Kingdom

(Received 5 November 2001; revised 7 January 2003; accepted 11 February 2003)

Pierce's formulation for the diffraction of spherical waves by a hard wedge has been extended to the case of the sound field due to a dipole source. The same approach is also used to extend a semiempirical model for sound propagation above an impedance discontinuity due to a dipole source. The resulting formulas have been validated by comparing their numerical solutions with that computed by summing the sound fields due to two closely spaced monopole sources of equal magnitude but opposite in phase. These new formulations are then used to develop a simple model for calculating the dipole sound field diffracted by a barrier above an impedance ground. Applications of these models relate to transportation noise prediction, particularly railway noise abatement, for which dipole sources are commonly used. The numerical predictions have been found to compare reasonably well with indoor measurements using piezoceramic transducers as dipole sources. © *2003 Acoustical Society of America.* [DOI: 10.1121/1.1566977]

PACS numbers: 43.28.En, 43.20.El [LCS]

I. INTRODUCTION

There is considerable interest in the study of noise reduction by means of screens and barriers in the context of environmental noise control. Although approximations for the calculation of the barrier insertion loss are widely used, the theoretical foundation for these studies is diffraction theory that is intimately related to corresponding solutions for electromagnetic fields.[1] An analytic solution for the sound field due to an omnidirectional point source diffracted by a hard wedge of arbitrary angle has been derived by Pierce.[2] It is often used as the basis for calculations of the screening effects due to barriers.[3] In addition, De Jong *et al.*[4] have developed a semiempirical solution for the calculation of the sound field above an admittance discontinuity, which is based on the diffraction of sound by a horizontal screen.

In view of the difficulties of computing Pierce's original solution[2] that includes Fresnel integrals, Hadden and Pierce[5] have reformulated the problem and propose an expression using simpler functions. However, more recently, Menounou *et al.*[6] have suggested a formulation of the diffraction integral by means of Hankel functions. Their approach considers the diffracted wave as being emitted by a directive line source located at the edge of the wedge. It leads to a unified formulation for the diffraction of the field due to point and line sources as well as arrays of point sources. In the case of an omnidirectional point source, it recovers Pierce's solution when asymptotic expressions are used.

The dipole field is a classical problem for the diffraction of electromagnetic waves,[1] but little can be found about the acoustic dipole and although, for example, train noise is modeled by means of a line of incoherent dipoles,[16–18] most of the methods for evaluating the shielding by barriers in the vicinity of tracks are approximations based on the solution for spherical or cylindrical waves.[18] The problem of diffraction of sound waves emitted by a dipole source has not been treated yet. Such a calculation is useful in the context of railway noise as well as for moving sources in general. It has been shown recently[7] that the sound field due to a monopole source in motion can be separated into two components: one that has the characteristics of a monopole and a second that has a dipolar behavior.

Our aim in this paper is to give a solution for the pressure field due to an arbitrarily oriented dipole diffracted by a wedge. This solution can then be used to extend De Jong's semiempirical model for propagation above an admittance step to dipole sources, as well as for the calculation of the sound field due to dipoles in the presence of barriers. Our starting point is the diffracted pressure for a monopole, as derived by Pierce.[2,8] This formulation is preferred to that given later by Hadden and Pierce[5] because of its consistency with De Jong's model[4] as well as the recent formulation of the Directive Line Source Model.[6]

The structure of the paper is as follows: in Sec. II we introduce the fundamental approach used to derive the sound field due to a dipole for the direct waves, reflected waves, and diffracted waves. In Sec. III, we discuss the use of these formulations for predicting sound in outdoor environments. Two typical cases are considered. They are namely, (1) sound propagation above an impedance discontinuity and (2) sound propagation in the presence of a barrier above the ground. In Sec. IV we present the experimental results for the validation of our theoretical formulations. Finally, Sec. V summarizes the main results obtained in the paper.

[a]On leave from the Department of Mechanical and Environmental Engineering, The Open University, Walton Hall, Milton Keynes MK7 6AA, United Kingdom.
[b]Author to whom correspondence should be addressed. Electronic mail: mmkmli@polyu.edu.hk

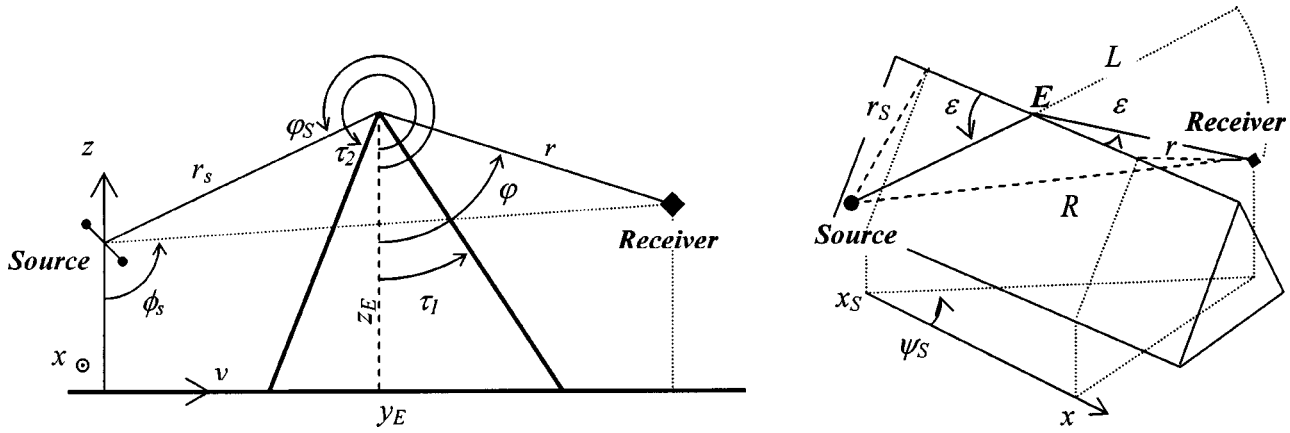

FIG. 1. Geometry for a wedge of arbitrary shape.

II. THEORETICAL FORMULATION

A. Geometrical configuration

Consider a two-dimensional wedge that has a constant cross-sectional area in the *y*-*z* plane and an arbitrary top angle $T=\tau_2-\tau_1$. The angles τ_1 and τ_2 are measured from the positive *z* axis; see Fig. 1. The wedge is acoustically hard with two reflecting planes. We choose a rectangular coordinate system such that the vertical *z* axis passes through the center of the source. The edge of the wedge is located in the direction parallel to the *x* axis and it is situated a horizontal distance of y_e and a height of z_e from the origin. In some situations, it may be more convenient to use a cylindrical polar coordinates system (r, φ, x) to specify field points from the edge of the wedge. These two coordinate systems are related according to

$$r=\sqrt{(y-y_e)^2+(z-z_e)^2}, \tag{1a}$$

$$\varphi=-\arctan\left(\frac{y-y_e}{z-z_e}\right), \tag{1b}$$

$$y=y_e+r\sin\varphi, \tag{1c}$$

$$z=z_e-r\cos\varphi, \tag{1d}$$

where the angle φ is measured from the vertical *z* axis. In the cylindrical polar coordinate system, the two sides of the wedge are located at $\varphi=\tau_1$ and $\varphi=\tau_2$. Defining a wedge index,[2]

$$\nu=\frac{\pi}{\tau_2-\tau_1}, \tag{2}$$

we can fix the shape of the wedge by specifying the parameters, ν, τ_1, and z_e.

To derive an analytical expression for the sound field due to a dipole source, it is useful to identify the source orientation by its direction cosines (ℓ_x,ℓ_y,ℓ_z) in the rectangular coordinate system as follows:

$$\begin{aligned}\ell_x&=\sin\gamma\cos\psi,\\ \ell_y&=\sin\gamma\sin\psi,\\ \ell_z&=\cos\gamma,\end{aligned} \tag{3}$$

where γ and ψ are the polar and azimuthal angles as shown in Fig. 2.

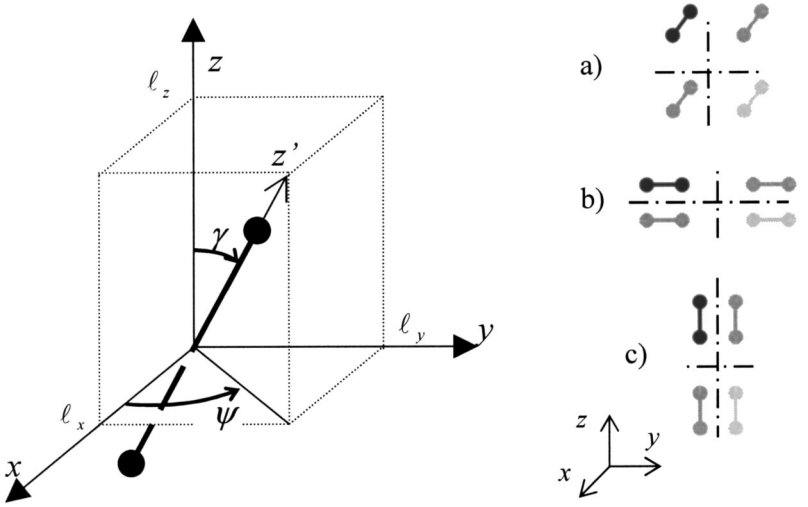

FIG. 2. Dipole orientation and direction cosines and relative orientations of a horizontal (a) along the *x* axis, (b) along the *y* axis, and vertical dipoles (c), and their images with respect to the horizontal and vertical planes.

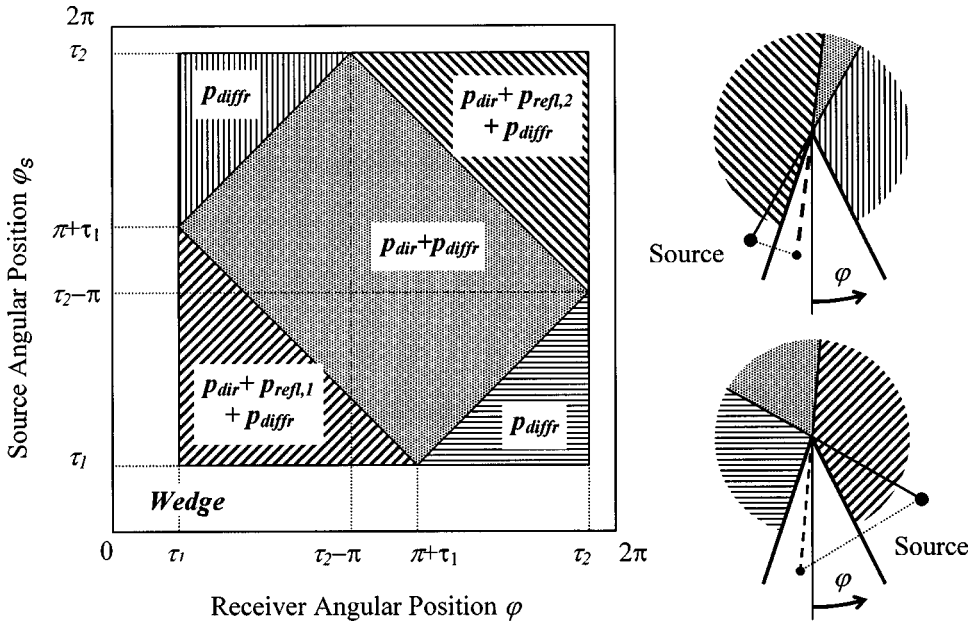

FIG. 3. Components of the pressure field in a function of the relative source and receiver positions with the faces of a wedge (τ_1 and τ_2).

B. The sound field in the vicinity of an acoustically hard wedge

The sound field can be expressed as a sum of four components: the direct wave term, two terms corresponding to the waves reflected by the planes at either sides of the wedge, and the diffracted wave as follows:

$$p_{\text{tot}} = p_{\text{dir}} + p_{\text{refl},1} + p_{\text{refl},2} + p_{\text{diffr}}. \tag{4}$$

The first three components of the total pressure may vanish depending on the source and receiver positions relative to the obstacle. The presence or absence of these components has been extensively discussed in the literature[2,5] and is summarized in Fig. 3.

The pressure field due to a dipole can be derived by considering its definition: it is the total field due to two monopoles of equal strength but 180° out of phase, infinitely close to one another.[8] The resultant sound field is given by

$$p = \lim_{|\Delta|\to 0} \frac{p_0(\mathbf{R},\mathbf{R_S}+\Delta) - p_0(\mathbf{R},\mathbf{R_S}-\Delta)}{2|\Delta|}, \tag{5a}$$

where p_0 is the pressure field due to a monopole, $\mathbf{R}$ and $\mathbf{R_S}$ are, respectively, the receiver and source coordinate vectors and the vector Δ represent the separation between the two out-of-phase monopoles, including the dipole orientation:

$$\Delta = |\Delta| \begin{pmatrix} \ell_x \\ \ell_y \\ \ell_z \end{pmatrix}. \tag{5b}$$

Consider a coordinate system (x',y',z') with the z' axis laying along the dipole axis, as illustrated in Fig. 2, Eq. (5a) can be rewritten as

$$p = \lim_{|\Delta|\to 0} \frac{p_0(x',y',z',x's,y's,z's+|\Delta|) - p_0(x',y',z',x's,y's,z's-|\Delta|)}{2|\Delta|}$$

$$= \frac{\partial p_0(x',y',z',x's,y's,z's)}{\partial z's} = \left(\frac{\partial xs}{\partial z's}\frac{\partial}{\partial xs} + \frac{\partial ys}{\partial z's}\frac{\partial}{\partial ys} + \frac{\partial zs}{\partial z's}\frac{\partial}{\partial zs} \right) p_0(\mathbf{R},\mathbf{R_S}). \tag{5c}$$

(ℓ_x,ℓ_y,ℓ_z) are the direction cosines for the z' axis and hence express (x,y,z) as functions of z'; Eq. (5c) can then be rewritten as

$$p = (\mathbf{I}\cdot\nabla_{\mathbf{S}}) p_0(\mathbf{R},\mathbf{R_S}),$$

$$\text{with } (\mathbf{I}\cdot\nabla_{\mathbf{S}}) = \left[\ell_x \frac{\partial}{\partial x_S} + \ell_y \frac{\partial}{\partial y_S} + \ell_z \frac{\partial}{\partial z_S} \right]. \tag{6}$$

C. Direct and reflected waves

The direct wave from a dipole source is well known as it is the free field solution,[8–10]

$$p_{\text{dir}} = P_0 \Theta_R \frac{1-ikR}{R^2} e^{ikR}, \tag{7a}$$

where P_0 is a pressure magnitude constant. Θ_R and R are,

respectively, directivity factor and the direct path given by

$$\Theta_R = -(\mathbf{l}\cdot\nabla_S)R$$
$$= \cos\gamma\cos\phi_S + \sin\gamma\sin\phi_S\cos(\psi_S-\psi), \tag{7b}$$
$$R = \sqrt{(x-x_S)^2+(y-y_S)^2+(z-z_S)^2}. \tag{7c}$$

The directivity factor is a function of the dipole orientation and the relative source and receiver position represented here by the incidence angle ϕ_S and the azimuthal angle ψ_S (see Fig. 1). It is interesting to note that the pressure falls as $1/R^2$ for $kR \ll 1$ and $1/R$ for $kR \gg 1$. The expressions of the directivity factor Θ_R and the direct path R can be written in the cylindrical coordinate system (r, φ, x) as follows:

$$\Theta_R = \ell_x\frac{x-x_S}{R} + \ell_y\frac{r\sin\varphi - r_S\sin\varphi_S}{R}$$
$$-\ell_z\frac{r\cos\varphi - r_S\cos\varphi_S}{R}, \tag{8a}$$
$$R = \sqrt{r^2+r_S^2-2rr_S\cos(\varphi-\varphi_S)+(x-x_S)^2}. \tag{8b}$$

The reflected waves can be calculated using a local coordinates system relative to each face of the wedge. It is then straightforward to calculate these waves in the case of a hard wedge. The sound fields due to these two components can be written in a compact form as

$$p_{\text{refl},n} = P_0\Theta_n\frac{1-ikS_n}{S_n^2}\exp(ikS_n), \tag{9a}$$

where $n=1, 2$ with the corresponding directivity factors and reflected wave paths given by

$$\Theta_n = \ell_x\frac{x-x_S}{S_n} + \ell_y\frac{r\sin\varphi + r_s\sin(\varphi_S-2\tau_n)}{S_n}$$
$$-\ell_z\frac{r\cos\varphi - r_s\cos(\varphi_S-2\tau_n)}{S_n} \tag{9b}$$
$$S_n = \sqrt{r^2+r_S^2-2rr_S\cos(\varphi+\varphi_S-2\tau_n)+(x-x_s)^2}. \tag{9c}$$

D. Diffracted wave

The wave diffracted at the edge of the wedge from a dipole source can be derived from the corresponding expression for a monopole source. Making use of Eq. (6) for the calculation of dipole fields, the diffracted pressure from a dipole source can be written as

$$p_{\text{diffr}} = (\mathbf{l}\cdot\nabla_S)D_0(\mathbf{R},\mathbf{R_S}), \tag{10}$$

where D_0 is the diffracted pressure for a monopole. Using Pierce's solution,[2] we can write the analytical solution for the diffracted pressure from a monopole source as

$$D_0 = P_0\frac{1+i}{2}\frac{\exp(ikL)}{L}[A_D(X_+)+A_D(X_-)], \tag{11a}$$

where L is the shortest path from the source to the diffraction edge to receiver,

$$L = \sqrt{(x-x_S)^2+(r+r_S)^2}. \tag{11b}$$

$A_D(X)$ is the diffraction integral:

$$A_D(X) = \frac{1}{\pi\sqrt{2}}\int_{-\infty}^{\infty}\frac{e^{-u^2}}{(\pi/2)^{1/2}X - e^{-i\pi/4}u}\,du$$
$$= \text{sgn}(X)[f(|X|) - ig(|X|)], \tag{11c}$$

where $f(X)$ and $g(X)$ are the auxiliary Fresnel functions.[2,11] The parameters, X_+ and X_-, are given by

$$X_- = \Gamma M_\nu(\alpha_-); \quad \alpha_- = \varphi - \varphi_S, \tag{11d}$$
$$X_+ = \Gamma M_\nu(\alpha_+); \quad \alpha_+ = \varphi + \varphi_S - 2\tau_1, \tag{11e}$$

with

$$\Gamma = \sqrt{krr_S/\pi L} = \sqrt{2rr_S/\lambda L} \tag{11f}$$

and

$$M_\nu(\alpha) = \frac{\cos\nu\pi - \cos\nu\alpha}{\nu\sin\nu\pi}, \tag{11g}$$

where λ is the wavelength. It is remarkable from Eqs. (11d) and (11e) that the term in X_- in the expression of the diffracted pressure in Eq. (11a) is related to the direct wave, whereas the term in X_+ is linked to the image source with respect to the wedge.

The presence of the sign function sgn(X) in Eq. (11c) means that the diffracted pressure for a monopole is not continuous. Mathematically speaking, its derivative is undefined at the points where X_+ and X_- are equal to 0. These points are the lines of sight for the direct and reflected waves. However, the total pressure field is continuous. The step in the diffracted pressure is then compensated for by the presence (or absence) of the direct or reflected wave considered and the value of the diffracted pressure on the sight lines can be calculated using the continuity of the total pressure. Before we proceed, we remark that De Jong[4] gives a slightly different formulation for the diffracted pressure due to a monopole source, making use of another form of Fresnel function than the diffraction integral A_D. Although it requires tedious manipulations on the Fresnel integrals, it is straightforward to show that this expression for the diffracted pressure wave is actually identical to Pierce's formulation.[2]

Next, we wish to derive an analytical expression for the diffracted wave due to a dipole source. As shown in Fig. 1, let ε be the angle made by the diffracted ray with the diffraction edge. According to Keller's law of diffraction, this angle is the same for both parts of the diffracted ray path[8] (source to edge and edge to receiver); thus

$$\cos\varepsilon = (x-x_S)/L \tag{12a}$$

and

$$\sin\varepsilon = (r+r_S)/L. \tag{12b}$$

The derivative of the auxiliary Fresnel functions $f(X)$ and $g(X)$ are[11]

$$f'(X) = -\pi Xg(X), \tag{13a}$$
$$g'(X) = \pi Xf(X) - 1. \tag{13b}$$

Hence, the diffracted wave for an arbitrarily oriented dipole can be derived by substituting Eqs. (11), (12a), (12b), (13a), and (13b) into Eq. (10):

$$p_{\text{diffr}} = P_0 \frac{1+i}{2} \Theta_L \frac{1-ikL}{L} \frac{e^{ikL}}{L} [A_D(X_+) + A_D(X_-)]$$
$$- P_0 \frac{1-i}{2} \frac{\exp(ikL)}{L} [1 - \pi X_- A_D(X_-)]$$
$$\times \left\{ \frac{X_-}{2} \left[\frac{\Theta_L}{L} + \frac{\sin\varphi_S - \cos\varphi_S}{r_S} \right] - X'_- \frac{\cos\varphi_S + \sin\varphi_S}{r_S} \right\}$$
$$- P_0 \frac{1-i}{2} \frac{\exp(ikL)}{L} [1 - \pi X_+ A_D(X_+)]$$
$$\times \left\{ \frac{X_+}{2} \left[\frac{\Theta_L}{L} + \frac{\sin\varphi_S - \cos\varphi_S}{r_S} \right] + X'_+ \frac{\cos\varphi_S + \sin\varphi_S}{r_S} \right\}, \tag{14a}$$

where Θ_L, which is the directivity factor at the point where the diffracted ray intersects the edge of the wedge, is given by

$$\Theta_L = -(\mathbf{l}\cdot\boldsymbol{\nabla}_\mathbf{S})L = \ell_x \cos\varepsilon - (\ell_y \sin\varphi_S - \ell_z \cos\varphi_S)\sin\varepsilon. \tag{14b}$$

The parameters, X'_- and X'_+, can be determined according to

$$X'_\pm = \Gamma M'_\nu(\alpha_\pm), \tag{14c}$$

where M'_ν is the derivative of M_ν with respect to its argument $\alpha_\pm$.

At high frequencies and long ranges with respect to the wavelength considered, Γ and hence $X'_\pm$ are large and the auxiliary Fresnel functions can be approximated by

$$f(X) \approx 1/\pi X, \tag{15a}$$

$$g(X) \approx 0. \tag{15b}$$

Therefore, the diffraction integral of Eq. (11c) reduces to

$$A_D(X) = \text{sgn}(X)[f(|X|) - ig(|X|)] \approx 1/\pi X. \tag{15c}$$

Figure 4 shows that for arguments greater than 1, the approximation in Eq. (15c)—shown by the dotted line—is already acceptable. The fact that $A_D(X)$ is an odd function ensures the same results for negative values of X. At high frequencies and long ranges with respect to the wavelength, the diffracted pressure as expressed in Eq. (14a) can be approximated by

$$p_{\text{diffr}} \approx P_0 \frac{1+i}{2} \Theta_L \frac{1-ikL}{L} \frac{e^{ikL}}{L} [A_D(X_+) + A_D(X_-)]. \tag{16}$$

The expression in Eq. (16) is analogous to the expression for a monopole source, but modified by the source strength factor $(1-ikL)/L$ and the directivity factor Θ_L, both typical of a dipole. Menounou's Directive Line Source Model[6] leads to a rather similar result for an array of two sources. Nevertheless, the source strength factor $(1-ikL)/L$ must then be introduced to account for the 180° difference in phase of the two point sources composing the dipole.

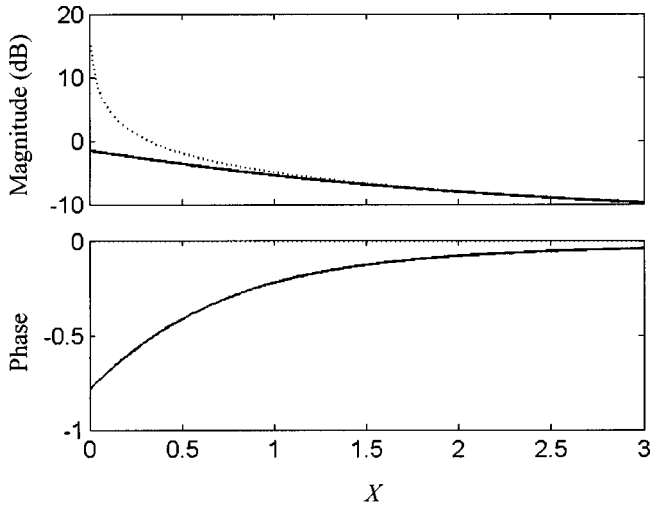

FIG. 4. Approximation of the diffraction integral $A_D(X)$ by $1/\pi X$. The exact function is shown by solid lines, its approximation represented by dotted lines.

E. Diffraction by a half-plane

A common idealization of diffraction of sound due to outdoor noise source by a barrier is that of diffraction by a thin screen, modeled by a half-plane. Diffraction by a half-plane is a classical case and can be derived by considering an infinitely thin wedge of top angle $T=0$. Hence,

$$\tau_1 = 0; \quad \tau_2 = 2\pi \quad \text{and} \quad \nu = 1/2. \tag{17}$$

The function M_ν used for the calculation of the diffracted wave can then be rewritten from Eq. (11g) as

$$M_\nu(\alpha) = -2\cos(\alpha/2). \tag{18}$$

The total sound field can be computed for a given source/receiver geometry. In Fig. 5, we show the total sound field at 1000 Hz when the receiver revolves around the edge of a half-plane. The source is located 1 m away from the edge, at $\varphi_S = 5\pi/3$ and its image is thus located at $\varphi'_S = \pi/3$ (both are marked by stars in Fig. 5). The receiver revolves at 2 m from the edge of the half-plane ($r = 2$ m). These plots show the sound field for a monopole (dotted line), a horizontal dipole (solid line), and a vertical dipole (dashed line). We remark that the axis of the horizontal dipole, which is aligned along the y axis, is perpendicular to the edge of the half-plane. Relative sound pressure levels (SPL) are used to facilitate the presentation of the theoretical results. The corresponding reference levels for different source types are chosen with the receiver located on the non-illuminated side of the half-plane at the given range, i.e., 2 m from the edge. The continuity of the total sound field on the sight lines for direct and reflected waves, marked by radial lines, is evident in the plots for all source types.

To confirm the validity of Eq. (14a) for the diffracted sound field, comparisons are made with numerical calculations using two monopoles of 180° difference in phase and very close to one another. In Fig. 5, we display these predicted results with squares for the sound field due to the horizontal dipole and triangles for that due to the vertical

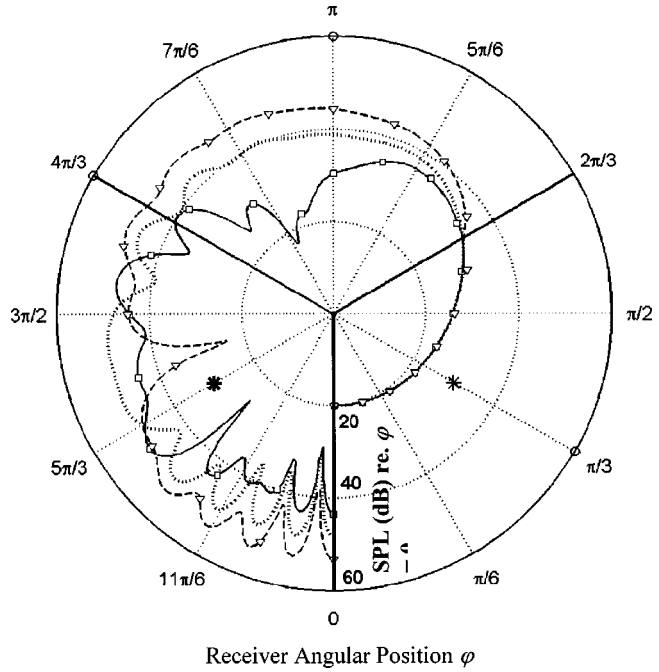

FIG. 5. The total sound field at 1000 Hz around a half-plane ($\nu=1/2$; $\tau_1=0$; $\tau_2=2\pi$) for a receiver revolving around the edge at $r=2$ m. The source is located at $\varphi_S=5\pi/3$; $r_S=1$ m; $x=x_S=0$. Three different sources are shown: a horizontal dipole (solid line), a vertical dipole (dashed line), and a monopole (dotted line). The squares and the triangles show the calculations for two monopoles with 180° out of phase and close to one another in the configuration of a horizontal and a vertical dipole, respectively. The stars show the positions of the source and its image with respect to the left-hand side of the screen. The results are referenced to the SPL when the receiver is located on the nonilluminated side of the wedge ($\varphi=\tau_1$). Solid radii represent the sight lines for direct and reflected waves.

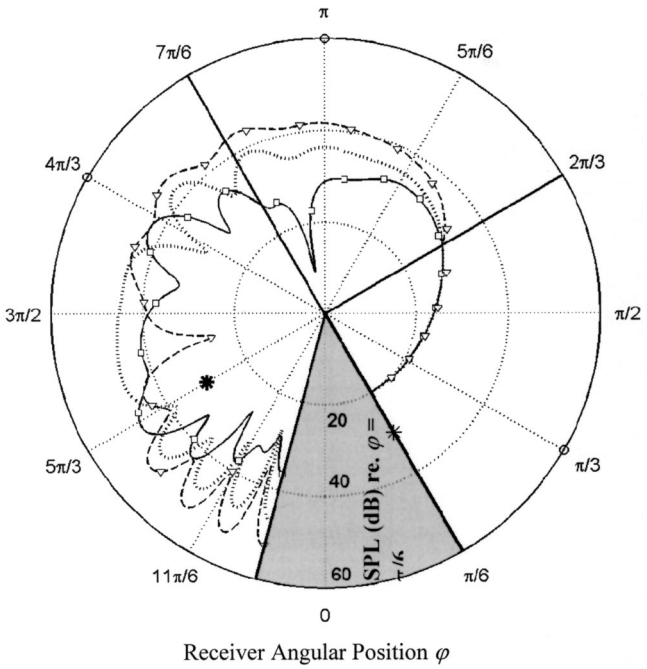

FIG. 6. The same as Fig. 5, but for a wedge of top angle $\pi/4$ ($\nu=4/7$; $\tau_1=\pi/6$; $\tau_2=23\pi/12$).

dipole. The predictions with such ''composite dipoles'' show no discernable difference with waves calculated by Eq. (14a).

In the shadow zone, all sources present the same variations in diffracted pressure, as the directivity function Θ_L is calculated at the top edge of the obstacle and is therefore independent of the receiver angular position. Outside the shadow zone, where the diffracted wave interferes with the direct wave, it is remarkable that the sound field pattern for a vertical dipole is comparable in shape to that of a monopole. This is not the case for the horizontal dipole. Different but related observations were made in the case of propagation of sound due to a dipole above ground.[10] In this case, the sound field due to a horizontal dipole (whose image has the same orientation) is very close to that due to a monopole. On the other hand, the sound field due to a vertical dipole above the ground (whose image is inverted) is somewhat different because of further interference between direct and reflected waves as well as a loss of reciprocity. Conversely, in the presence of a vertical half-plane described here, the image of the vertical dipole conserves the source orientation, whereas that of a horizontal dipole is inverted. Relative orientations of dipole sources and their images are summarized in Fig. 2. We have seen in Sec. II D that the source and its image both contribute to the diffracted pressure and hence their orientations have an important influence on its interaction with direct and reflected pressure waves.

Figure 6 displays the total sound field around the edge of a hard wedge of top angle $\pi/4$ ($\nu=4/7;\tau_1=\pi/6;\tau_2=23\pi/12$) at 1000 Hz for the same source and receiver positions. For such a narrow wedge, the pattern for a vertical dipole is again closer in shape to that of the monopole, due to the respective orientations of the source and its image. The continuity of pressure at the lines of sight is evinced and the agreement with the sound fields due to ''composite dipoles'' (squares for a horizontal dipole and a triangle for a vertical dipole) is again excellent.

Figure 7 shows the sound field for the same wedge and the same source as a function of the source–receiver offset distance $x-x_S$ for three receivers in different regions for the composition of the total pressure field. These receiver positions are shown by circles in Fig. 6. Predictions are shown for two horizontal dipolesed—along the x axis, parallel to the edge of the wedge (dashed–dotted line), and along the y axis, perpendicular to the edge of the wedge (solid line), respectively. Also shown are predictions for a vertical dipole along the z axis (dashed line) as well as a monopole (dotted line). The dipole fields are compared with the corresponding ''composite dipoles'' (crosses, squares and triangles, respectively). The agreement is again very good. The plots have been normalized to the point of null offset, except for the dipole along the x axis as the receiver is then in the midplane of the dipole and there is no sound field.

The results for horizontal and vertical dipole are undistinguishable. These calculations confirm observations made in earlier studies,[6] stating that the diffracted wave show greater directivity in the transverse direction than waves from the original source in the absence of a barrier. This is due to the behavior of the diffraction integral $A_D(X)$. Its

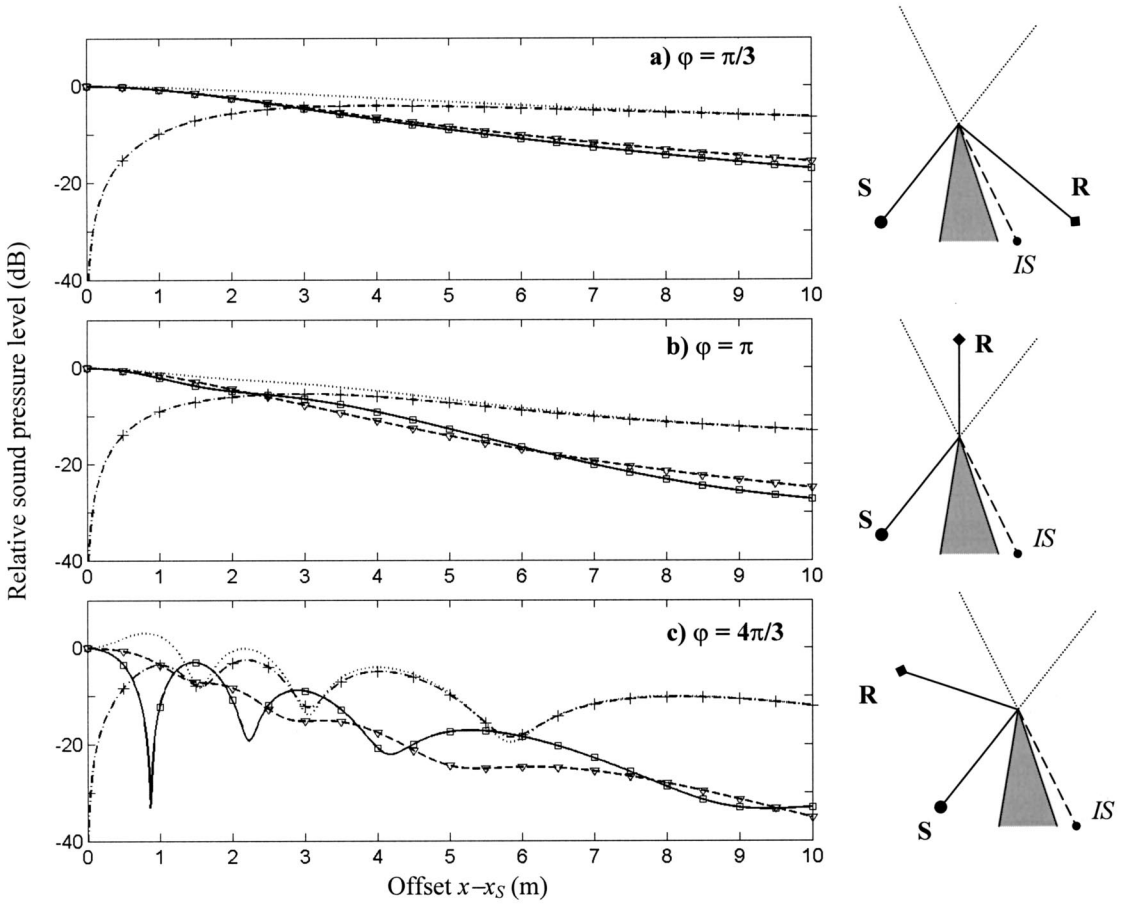

FIG. 7. The sound field at 1000 Hz in the presence of a hard wedge of top angle $\pi/4$ ($\nu=4/7$; $\tau_1=\pi/6$; $\tau_2=23\pi/12$) as a function of the source–receiver offset. The source is located at $r_S=1$ m; $\varphi_S=5\pi/3$. The receiver is located at $r=2$ m and at three positions corresponding to different compositions for the total pressure: (a) $\varphi=\pi/3$ (diffracted wave only); (b) $\varphi=\pi$ (direct wave and diffracted wave); and (c) $\varphi=4\pi/3$ (direct wave, wave reflected on the τ_2 side and a diffracted wave). These positions are shown in Fig. 6 by circles. Four different sources are shown: a horizontal dipole oriented along the y axis, perpendicular to the edge of the wedge (solid line), a horizontal dipole oriented along the x axis, parallel to the edge of the wedge (dashed–dotted line), a vertical dipole (dashed line), and a monopole (dotted line). The squares, the crosses, and the triangles show the calculations for two monopoles out of phase and close to one another in the configuration of the respective dipoles. The relative sound pressure level is referenced to its value at the point of null offset, except for the dipole along the x axis.

magnitude increases with offset, as X_- and X_+ decrease [cf. Eqs. (11d)–(11f) and Fig. 4]. This partly compensates for the decay in the sound field due to the increase in the source–receiver range. Outside the short offset range, the dipole along the x axis behaves in a way very similar to that of a monopole.

Comparing Figs. 7(a), (b), and (c) provides good insight into the influence of the direct waves and the reflections from the sides of the wedge on the total sound field. An interference pattern is observed in the region where the three components of the sound field are present. The horizontal dipole aligned along the x axis (dashed–dotted line) and the vertical dipole (dashed line) behave similarly to a monopole (dotted line) in that respect, whereas the pattern for the dipole aligned along the y axis (solid line) seems to be somewhat out of phase. This is also due to the relative orientations of the actual and image sources (see Fig. 2), which are identical for the dipole along x, almost the same for a vertical dipole and quasi-opposite for the dipole along the y axis. This figure shows that reflected waves are critical components of the total sound field.

III. TWO APPLICATIONS RELEVANT TO OUTDOOR ENVIRONMENT

A. Sound propagation above an admittance discontinuity

Several models can be found in the literature concerning the propagation of sound above a discontinuous ground. Boulanger *et al.* have given a review of these models.[12] Two of them are of interest for the present study as they make use of the solution for the diffracted pressure by a wedge. Koers' model[13] considers a wedge of top angle 180° with different admittance of each ''side.'' However, not only is such a model subject to the restrictions concerning the absorbent wedge but the sound field is not well defined when the reflection occurs at the point of discontinuity. The second model, a semiempirical one, has been proposed by De Jong.[4] It is based on the superposition of two half-planes of different admittance. The actual diffracted wave is then estimated by considering the two limiting cases: that of a hard screen in the air and that of homogeneous ground. De Jong's model has proved to give relatively good agreements with experi-

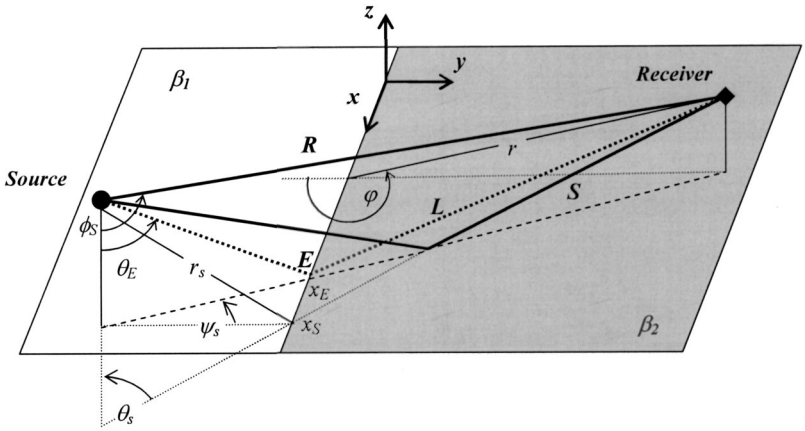

FIG. 8. Geometry for the propagation of sound above an admittance step.

mental results and with more accurate numerical calculations[12] for an omnidirectional point source. Having derived an expression for the pressure field due to a dipole diffracted by a half-plane, we shall now adapt De Jong's model to dipole sources.

After Li *et al.*,[10] the sound field due to an arbitratrily oriented dipole above a plane of specific normalized admittance β can be expressed in a close-form analytical solution as

$$p=\Theta_R\left[\frac{1-ikR}{R}\right]\frac{e^{ikR}}{R}+\Theta_S R_P\left[\frac{1-ikS}{S}\right]\frac{e^{ikS}}{S}+\Theta_Z(1-R_P)F(w)\left[\frac{1-ikS}{S}\right]\frac{e^{ikS}}{S}, \tag{19a}$$

where R and S are the direct and reflected ray paths, R_P is the plane wave reflection coefficient,

$$R_P=\frac{\cos\theta_S-\beta}{\cos\theta_S+\beta}, \tag{19b}$$

with θ_S the incidence angle of the reflected ray. The boundary loss factor, $F(w)$, is

$$F(w)=1+i\sqrt{\pi}we^{-w^2}\,\mathrm{erfc}(-iw), \tag{19c}$$

with the numerical distance w given by

$$w=(\tfrac{1}{2}ikS)^{1/2}(\cos\theta_S+\beta). \tag{19d}$$

The corresponding directivity factors are determined by

$$\Theta_R=\cos\phi_S\cos\gamma+\sin\phi_S\sin\gamma\cos(\psi_S-\psi), \tag{20}$$

$$\Theta_S=\cos\theta_S\cos\gamma+\sin\theta_S\sin\gamma\cos(\psi_S-\psi), \tag{21}$$

$$\Theta_Z=-\beta\cos\gamma+\sqrt{1-\beta^2}\sin\gamma\cos(\psi_S-\psi), \tag{22}$$

where ϕ_S is the elevation angle of the direct ray and ψ_S the azimuthal angle of the direct path connecting source and receiver shown in Fig. 8. The dipole orientation is defined by the polar and azimuthal angles γ and ψ (see Sec. II and Fig. 2).

In the presence of an admittance discontinuity on a flat reflecting ground (see Fig. 8), the pressure field for a monopole source of unit strength can be expressed as[4]

$$p_0=\frac{e^{ikR}}{R}+Q_r\frac{e^{ikS}}{S}+(Q_1-Q_2)D_0, \tag{23a}$$

where Q_1 and Q_2 are the spherical wave reflection coefficients calculated for the two types of ground,

$$Q_i=R_{p_i}+(1-R_{p_i})F(w_i),\quad \text{for } i=1,2, \tag{23b}$$

with R_{p_i} and w_i being the respective plane wave reflection coefficients and numerical distances. The parameter Q_r is the corresponding spherical wave reflection coefficient at the point of specular reflection and D_0 is the relative sound pressure of a monopole source diffracted by a horizontal half-plane with the edge coincided with the admittance discontinuity. The form of the solution for D_0 is given in a form similar to Eq. (11a) with a different configuration of source and receiver.

The sound field for a dipole of unit strength can be obtained by differentiating the expression for a monopole, the right hand side of Eq. (23a), to yield

$$p=(\mathbf{I}\cdot\nabla_\mathbf{S})\left[\frac{\exp(ikR)}{R}+Q_r\frac{\exp(ikS)}{S}\right]+(Q_1-Q_2)[(\mathbf{I}\cdot\nabla_\mathbf{S})D_0]+[(\mathbf{I}\cdot\nabla_\mathbf{S})(Q_1-Q_2)]p_{\mathrm{diffr}}, \tag{24}$$

where the operator $(\mathbf{I}\cdot\nabla_\mathbf{S})$ is given in Eq. (6) and p_{diffr} is the pressure due to the dipole source, diffracted by a horizontal half-plane whose edge coincides with the discontinuity,

$$p_{\mathrm{diffr}}\approx\frac{1+i}{2}\Theta_L\frac{1-ikL}{L}\frac{e^{ikL}}{L}[A_D(X_+)+A_D(X_-)], \tag{25a}$$

$$\Theta_L=\cos\theta_E\cos\gamma+\sin\theta_E\sin\gamma\cos(\psi_S-\psi), \tag{25b}$$

with L the diffracted ray pathlength. X_+ and X_- are defined in Eqs. (11d) and (11e) with angle φ_S measured from the negative y axis, as shown in Fig. 8. The parameter Θ_L is the directivity factor at the point E where the diffracted ray intersects the admittance discontinuity, i.e., the edge of the half-plane, as shown in Fig. 1. The parameters θ_E and ψ_S are, respectively, the elevation angle and azimuthal angle of the diffracted ray path joining source to edge to receiver.

The first bracketed term on the right hand side of Eq. (24) represents sound fields due to a dipole above the ground. Use can be made of the solution derived by Li *et al.*[10] shown in Eq. (19). The derivative of the diffracted pressure in the second term on the right-hand side of Eq. (24)

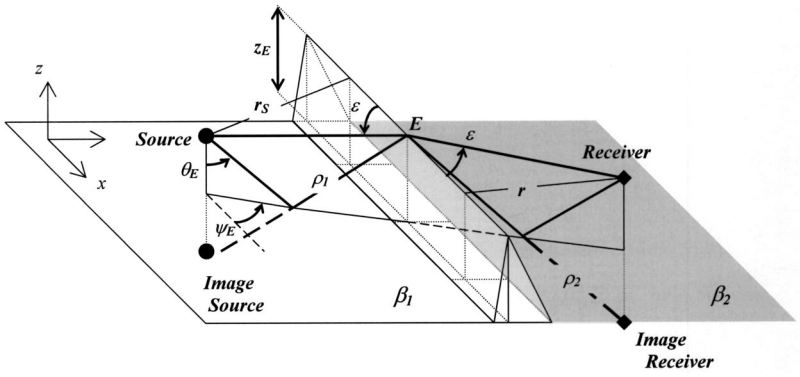

FIG. 9. Geometry for the propagation of sound in the presence of a barrier above the ground.

is the pressure due to a dipole source diffracted by a horizontal half-plane, cf. Eq. (16), with the use of appropriate parameters. The last term involves the derivative of the spherical wave reflection coefficients. In the case of a horizontal dipole, its contribution will not be significant compared with the first two terms because the variations of this reflection coefficient with horizontal distance are small. On the other hand, its influence becomes crucial in the case of a vertical dipole as the spherical wave coefficient is more sensitive to variations in height.

Li's formulation[10] is used to rewrite $(\mathbf{I}\cdot\nabla_{\mathbf{S}})Q_i$ as

$$(\mathbf{I}\cdot\nabla_{\mathbf{S}})Q_i=(\Theta_{Zi}-\Theta_S)\frac{1-ikS}{S}(1-R_{Pi})F(w_i),$$

$$\text{for}\quad i=1,2, \tag{26}$$

where Θ_S, Θ_{Z1}, and Θ_{Z2} can be determined according to Eqs. (21) and (22). Hence, Eq. (24) becomes

$$p=\Theta_R\frac{1-ikR}{R}\frac{e^{ikR}}{R}+\Theta_S\frac{1-ikS}{S}Q_r\frac{e^{ikS}}{S}$$
$$+\frac{1+i}{2}\frac{e^{ikL}}{L}\left[\Theta_L\frac{1-ikL}{L}(Q_1-Q_2)+\frac{1-ikS}{S}(\xi_1-\xi_2)\right]$$
$$\times[A_D(X_-)+A_D(X_+)], \tag{27a}$$

where

$$\xi_i=(\Theta_{Zi}-\Theta_S)(1-R_{Pi})F(w_i),\quad i=1,2. \tag{27b}$$

For near-grazing propagation and soft grounds, further approximations can be used,[10] in Eq. (27b) to simplify ξ_1 and ξ_2 as follows:

$$\xi_i\approx-2\beta_i\cos\gamma F(w_i),\quad i=1,2. \tag{27c}$$

The solution is nonsingular and continuous where the point of specular reflection crosses over the admittance discontinuity because, at the transition point, $L=S$; $\Theta_L=\Theta_S$ and $X_+=0$, which leads to $A_D(0)=-(1-i)/2$. Hence, the continuity of the solution is ensured.

B. Sound propagation in the presence of a barrier above the ground

Consider sound propagation in the presence of a barrier when source and receiver are located on either sides of a barrier with the receiver located at the shadow zone above ground. The sound field for a monopole source can then be represented by the sum of four components (see Fig. 9) corresponding to each path from source to receiver, taking into account the effect of the ground reflections. The total sound field can be expressed as

$$p_0=p_{0,S-R}+Q_1p_{0,IS-R}+Q_2p_{0,S-IR}+Q_1Q_2p_{0,IS-IR}, \tag{28}$$

where the subscripts *S, R, IS, IR* stand for the source, the receiver, the image source and the image receiver, respectively. The parameters, Q_1 and Q_2 are the reflection coefficients for the waves reflected on the source side (ground admittance β_1) and on the receiver side (ground admittance β_2). It has been found[13] that these reflection coefficients should be calculated for the respective paths joining the image source to the edge of the wedge (ρ_1) and the edge to the image receiver (ρ_2). These are calculated from geometrical considerations (see Fig. 9) as

$$\rho_1=\frac{r_S}{\sin\varepsilon}\sqrt{1-\frac{4z_e}{r_S}\left(\cos\varphi_S-\frac{z_e}{r_S}\right)\sin^2\varepsilon}, \tag{29a}$$

$$\rho_2=\frac{r}{\sin\varepsilon}\sqrt{1-\frac{4z_e}{r}\left(\cos\varphi-\frac{z_e}{r_S}\right)\sin^2\varepsilon}. \tag{29b}$$

In the case of a dipole source, the expression for the sound field can be obtained by substituting Eq. (28) into Eq. (6). This leads to

$$p=(\mathbf{I}\cdot\nabla_{\mathbf{S}})p_{0,S-R}+Q_1[(\mathbf{I}\cdot\nabla_{\mathbf{S}})p_{0,IS-R}]$$
$$+Q_2[(\mathbf{I}\cdot\nabla_{\mathbf{S}})p_{0,S-IR}]+Q_1Q_2[(\mathbf{I}\cdot\nabla_{\mathbf{S}})p_{0,IS-IR}]$$
$$+[(\mathbf{I}\cdot\nabla_{\mathbf{S}})Q_1]p_{0,IS-R}+[(\mathbf{I}\cdot\nabla_{\mathbf{S}})Q_2]p_{0,S-IR}$$
$$+\{Q_1[(\mathbf{I}\cdot\nabla_{\mathbf{S}})Q_2][(\mathbf{I}\cdot\nabla_{\mathbf{S}})Q_1]Q_2\}p_{0,IS-IR}. \tag{30}$$

However, as the reflection coefficient Q_2 is calculated for the path joining the edge of the barrier to the receiver, it is independent of the source coordinates in the vertical plane, hence,

$$(\mathbf{I}\cdot\nabla_{\mathbf{S}})Q_2=0. \tag{31a}$$

The derivative of the reflection coefficient Q_1 may here again be estimated after Li's formulation for the sound field due to a dipole above the ground,[10]

$$(\mathbf{I}\cdot\nabla_{\mathbf{S}})Q_1=(\Theta_{Z1}-\Theta_{S1})\frac{1-ik\rho_1}{\rho_1}(1-R_{P1})F(w_1), \tag{31b}$$

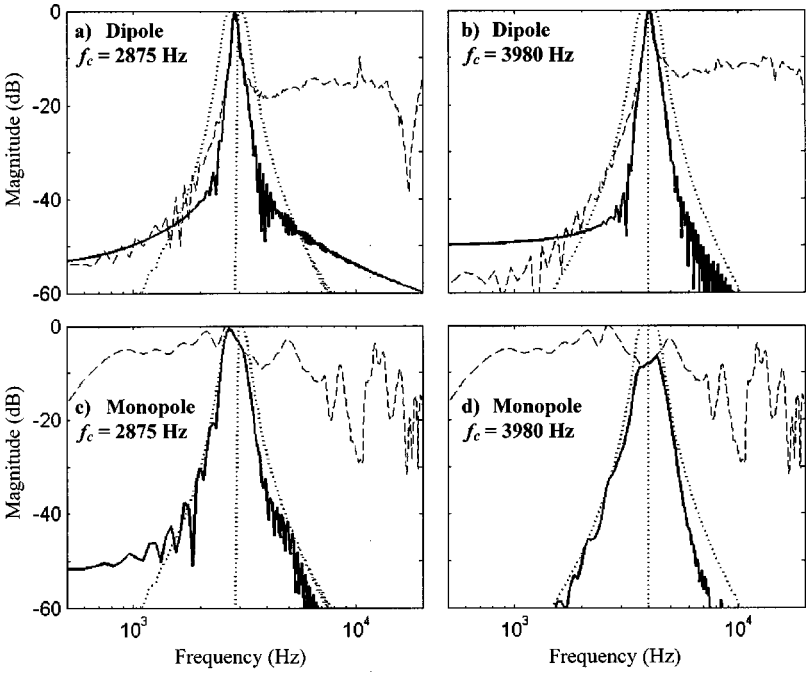

FIG. 10. Free field spectra of the sources used. The dashed lines show the broadband spectra, the solid lines the filtered spectra, and the dotted lines the third-octave band filters used. (a) Piezoceramic disk with resonant frequency $f_c = 2875$ Hz; (b) piezoceramic disk with $f_c = 3980$; (c) omnidirectional source, filtered on the third octave centered at $f_c = 2875$ Hz; (d) the same as (c) but for $f_c = 3980$ Hz.

where

$$R_{P1} = \frac{\cos\theta_E - \beta_1}{\cos\theta_E - \beta_1}, \tag{31c}$$

$$w_1 = (\tfrac{1}{2} ik\rho_1)^{1/2}(\cos\theta_E + \beta_1), \tag{31d}$$

$$\Theta_{S1} = \cos\theta_E \cos\gamma + \sin\theta_E \sin\gamma \cos(\psi_E - \psi), \tag{31e}$$

$$\Theta_{Z1} = -\beta_1 \cos\gamma + \sqrt{1-\beta_1^2} \sin\gamma \cos(\psi_E - \psi), \tag{31f}$$

with θ_E and ψ_E being the elevation and azimuthal angles of the path joining the image source to the edge of the barrier (see Fig. 9). Equation (30) can then be simplified to

$$p = p_{S-R} + Q_1 p_{IS-R} + Q_2 p_{S-IR} + Q_1 Q_2 p_{IS-IR} + (\Theta_{Z1} - \Theta_{S1})[p_{0,IS-R} + Q_2 p_{0,IS-IR}] \frac{1 - ik\rho_1}{\rho_1} \times (1 - R_{P1}) F(w_1), \tag{32}$$

where, when the receiver is in the shadow zone, p_{S-R}; p_{IS-R}; p_{S-IR}; p_{IS-IR} are the diffracted pressures for each of the four propagation paths calculated using the expression given in Eq. (16).

IV. LABORATORY MEASUREMENTS

A. Experimental setup

Measurements have been carried out in an anechoic chamber of dimension 6 m×6 m×4 m (high).

Piezoceramic disks with peak frequencies of 2875 Hz (diameter 35 mm) and 3980 Hz (diameter 27 mm) with dipole directivity have been used. Although they may be delicate to manipulate, similar disks were used successfully as dipole sources in our previous studies.[10] The impulse responses were obtained by means of a Maximum Length Sequence Analyzer[15] and then filtered on the third octave band centered on the peak frequency of the source. The sound pressure levels were then calculated by means of an integration of these filtered responses rather than on single frequencies, to ensure that small spectral instabilities linked to the change geometry do not affect the results presented here. Since the piezoceramic disks emitted quite low levels of sound, a relatively short source–receiver range up to 1.5 m was chosen in our indoor measurements. They also have been carried out with an omnidirectional source, a driver prolonged by a tube of diameter 30 mm and length 1.5 m. Here again the responses have been filtered on the third octave bands centered on the resonant frequencies of the dipole transducers. The sound pressure level is then calculated by integration of the filtered responses. The free field spectra of the various sources used are presented in Fig. 10.

The measurements were compared to theoretical predictions that have been adjusted with the filtered spectra of the corresponding sources. Hard ground was modeled by means of varnished plywood panels. Two different impedance grounds were modeled using a two-parameter model,[14] a carpet with equivalent parameters $\sigma_e = 10$ kPa s m^{-2} and $\alpha_e = 100$ m^{-1} and rough rubber mat sheets, with $\sigma_e = 8$ kPa s m^{-2} and $\alpha_e = 2000$ m^{-1}. Characterizations of these two materials by means of Excess Attenuation measurements are presented in Fig. 11. Barrier measurements have been made using a steel plate as a rigid thin screen.

B. Impedance discontinuity

In our experiments, the carpet and the rough rubber mat are used to create a mixed impedance ground surface. Figure 12 shows the variations of the sound pressure level with the percentage of the harder ground (rubber mat) on the source receiver path. The source height is 0.035 m above the rubber mat and the receiver height is 0.025 m. The source–receiver range is 0.75 m and there is no offset ($x_S = x = 0$). The data shown correspond to the measurements for a monopole (dots), a horizontal dipole along the y axis (squares), and a

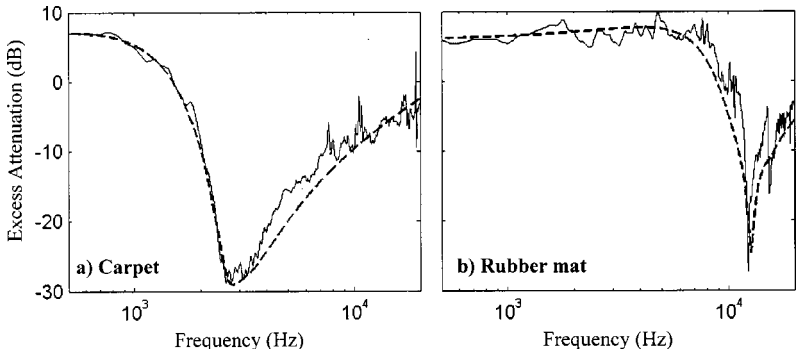

FIG. 11. Characterization of the two types of ground used. The solid lines show measurements for a separation of 0.75 m and source and receiver heights of 0.035 and 0.025 m, respectively, referenced to free field measurements. The dashed lines show predictions using a two-parameter ground model (Ref. 14) with the following values: (a) $\sigma_e = 10$ kPa s m^{-2}; $\alpha_e = 75$ m^{-1} for the carpet; (b) $\sigma_e = 8$ kPa s m^{-2}; $\alpha_e = 2000$ m^{-1} for the rubber mat.

vertical dipole (triangles). They are compared with the theory: the dotted line shows the predictions for the monopole, the solid line for the horizontal dipole, and the dashed line for the vertical dipole. The sound pressure levels have been normalized at the point of discontinuity in Figs. 12 and 13 in order to give a better comparison of the trends at this point, particularly in the change of slope observed when the surface on which the reflection occurs changes.

The continuity of the pressure field is well respected when the specular reflection occurs on the discontinuity line (about 58% of rubber mat on the source-receiver path). Nevertheless, we can observe a discrepancy in Fig. 12 between the theory and the measurements when the percentage of the harder ground tends to zero. This is also observed for a monopole source and may therefore be a fault inherent to De Jong's model. It is, however, slightly more important in the case of a dipole, probably due to the use of an approximate formula for the derivatives of the reflection coefficients. Outside this region, where the percentage of harder ground is larger, the agreement between measurements and theory is generally very good. There is a discrepancy between predictions of measurements for a vertical dipole in Fig. 12(b) for the range 50%–60% of hardest ground. In view of the good results obtained for other configurations this can be explained by a slight deviation in the orientation of the piezoceramic source used for the corresponding set of measurements.

As in the case of propagation above a homogeneous boundary,[10] we can observe from Fig. 12 that the behavior of the horizontal dipole is very similar to that of a monopole. The behavior of the vertical dipole is somewhat different. This can be explained, as mentioned earlier in Sec. II E, when commenting upon Fig. 5, by the relative orientations of the sources and their images.

Figure 13 shows the variations of the sound pressure level with source–receiver range. The source is at height 0.035 m above the rubber mat and 0.6 m away from the discontinuity ($y_e = 0; y_S = -0.6$ m). The receiver is located 0.025 m above the ground and its position varies from $y = -0.1$ m to $y = 0.9$ m. Here again, the sound field of a horizontal dipole (solid line) is almost indistinguishable from that due to a monopole (dotted line). The vertical dipole (dashed line) is more sensitive to the change in the value of the admittance, as one can observe a more important change of slope in the decrease of the sound pressure level with range when the specular reflection occurs on the second type of ground. The agreement with the experimental data for the three types of source (dots for monopole, squares and triangles for horizontal and vertical dipole, respectively) is again very good.

Figure 14 shows the variations of the sound pressure level for a horizontal dipole along the discontinuity (x axis) with the source–receiver offset $x - x_S$ (solid line for the theory and crosses for the experimental data). The results for a monopole are shown for comparison (dotted line: theory, dots: measurements). The source is 0.035 m above the rub-

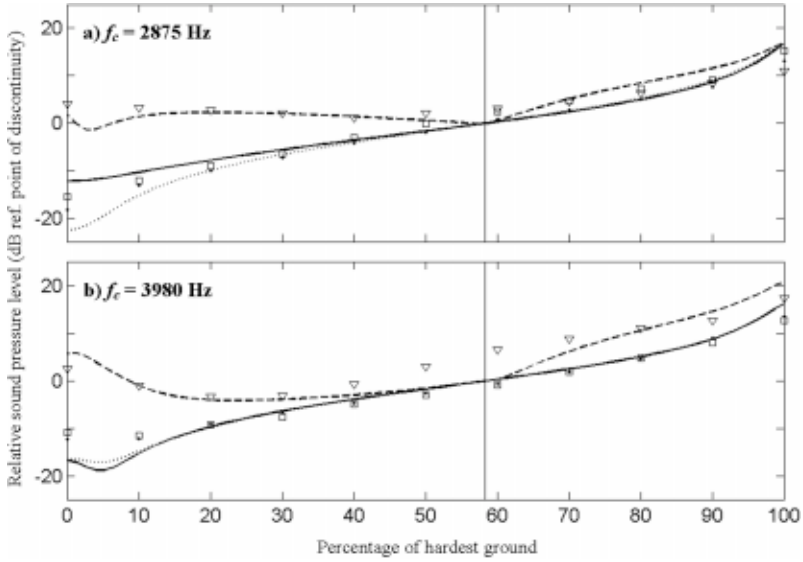

FIG. 12. Sound field above an admittance step for a monopole (dotted line for the theory; dots for the experimental data), a horizontal dipole (solid line: theory; squares: measurements) and a vertical dipole (dashed line: theory; triangles: measurements) as a function of the percentage of the hardest ground (rubber mat). The two ground models are those presented in Fig. 11. The source is located at height $z_s = 0.035$ m above the rubber mat, the receiver height is $z = 0.025$ m. The source–receiver range is $y - y_S = 0.75$ m and there is no offset ($x - x_S = 0$). The results are referenced to the predicted SPL at the point where the specular reflection occurs at the discontinuity (58% of harder ground), materialized by the vertical solid line.

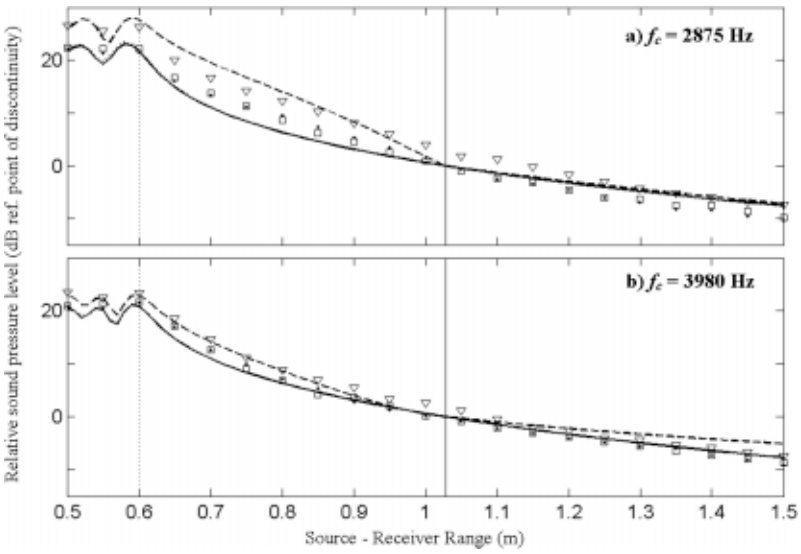

FIG. 13. Sound field above a rubber mat–carpet discontinuity for a monopole (dotted line for the theory; dots for the experimental data), a horizontal dipole (solid line: theory; squares: measurements) and a vertical dipole (dashed line: theory; triangles: measurements) as a function of the source–receiver range. The discontinuity is located at $y=0$. The source is located at height $z_S=0.035$ m above the rubber mat and at $y_S=-0.6$ m, the receiver at $z=0.025$ m. The source–receiver distance $y-y_S$ varies from 0.5 to 1.5 m and there is no offset ($x-x_S=0$). The results are referenced to the predicted SPL at the point where the specular reflection occurs at the discontinuity ($y-y_S=1.027$ m), materialized by the vertical solid line.

ber, 0.2 m away from the discontinuity and the receiver is 0.025 m above the carpet, 0.3 m away from the discontinuity. When there is no offset, there is no sound field, as the receiver is located in the midplane of the dipole source. The sound pressure level then increases with the offset following the directivity function of the source and reaches a stable value when the offset is roughly of the same order as the source–receiver distance as increases in the directivity index are compensated by longer ranges. Here again, the agreement in between the predictions and the experimental data is very good.

C. Barrier measurements

The study of the sound field in the presence of a barrier over the ground involves images with respect to the ground as well as the obstacle. This is particularly interesting in the light of the remarks we have made in Sec. II E.

Figures 15, 16, and 17 show the variations of the sound field with the receiver position when the ground is hard on both sides, hard on the source side and covered with carpet on the receiver side, and covered with carpet on both sides, respectively. The height of the screen is $z_e=0.22$ m and it is located at $y_e=0$. The source is located at $x_S=0$; $y_S=-0.3$ m; $z_S=0.1$ m and the receiver is located at $x=0$ and $z=0.05$ m. The dots show the experimental results for a monopole, the squares for a horizontal dipole along the y axis (perpendicular to the edge of the screen), and the triangles for a vertical dipole. They are compared with theoretical predictions with a dotted line for the monopole, a solid line for the horizontal dipole, and a dashed line for the vertical dipole. As in the case of the admittance discontinuity, the results shown here for the sound pressure level are based on an integration of the sound power over the third octave and centered at the resonant frequencies of the dipole sources (respectively, 2875 and 3980 Hz).

Agreement between the measurements and the predictions is very good. One may notice that, in the configuration chosen, the behavior of the dipoles is somewhat similar to that of the monopole, independently of the orientation. As we have mentioned in the beginning of this section, the image of the horizontal dipole with respect to the ground conserves the source orientation. This type of source behaves like a

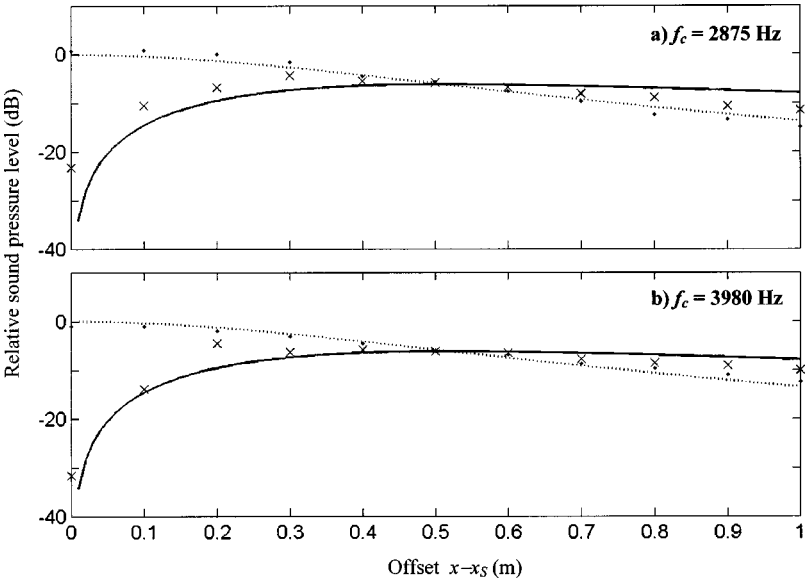

FIG. 14. Sound field above a rubber mat–carpet discontinuity for a monopole (dotted line for the theory; dots for the experimental data) and a horizontal dipole along the line of discontinuity (solid line: theory; squares: measurements) as a function of the offset $x-x_S$. The discontinuity is located at $y=0$. The source is located at $y_S=-0.2$ m, at height $z_s=0.035$ m above the rubber mat and the receiver at $y=0.3$ m, at height $z=0.025$ m above the carpet. The results for a monopole are referenced to the predicted SPL when there is no offset; those for the dipole are arbitrarily referenced.

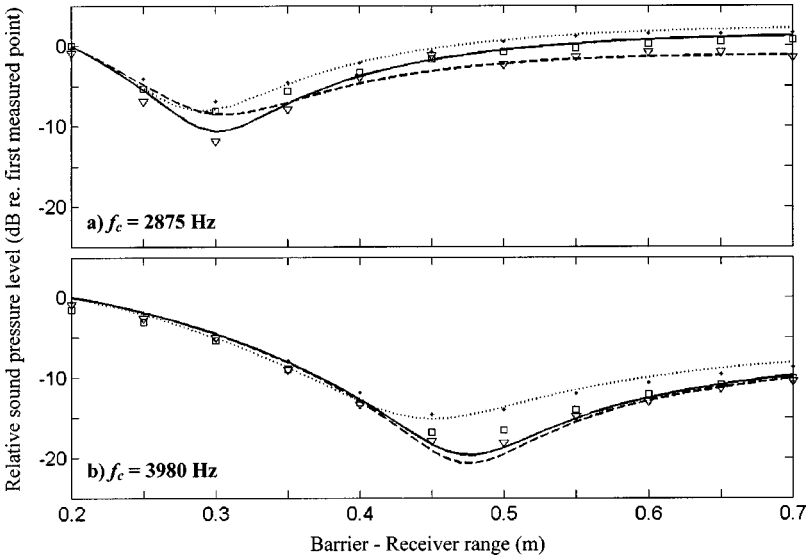

FIG. 15. Sound field diffracted by a rigid thin screen in the presence of ground for a monopole (dotted line for the theory; dots for the experimental data), a horizontal dipole (solid line: theory; squares: measurements) and a vertical dipole (dashed line: theory; triangles: measurements). The screen is located at $y_e=0$ and its height is $z_e=0.22$ m. The source coordinates are $x_S=0$; $y_S=-0.3$ m; $z_S=0.1$ m. The receiver is located at $x=0$ and $z=0.05$ m its distance from the barrier $y-y_e$ is the varying parameter. The ground on both sides is hard. The results are referenced to the total predicted SPL in the presence of the barrier at the first point considered ($y-y_e=0.2$ m).

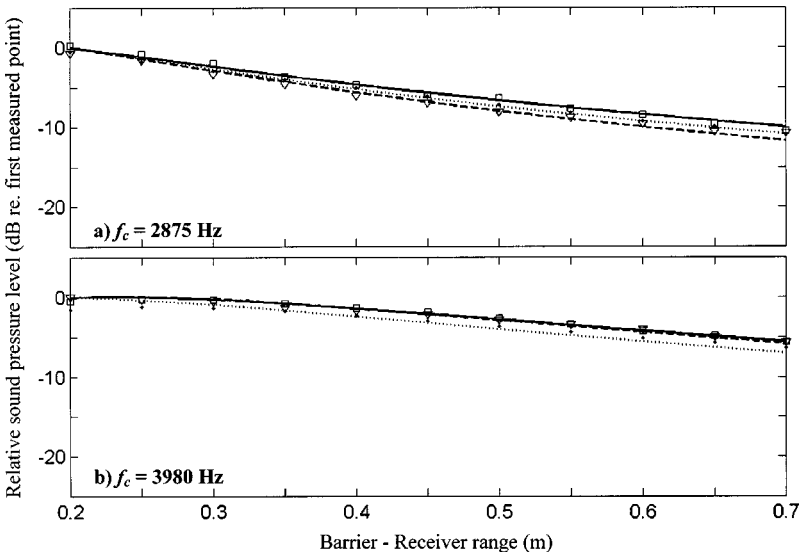

FIG. 16. The same as Fig. 15, except the ground is hard on the source side and covered with carpet on the receiver side.

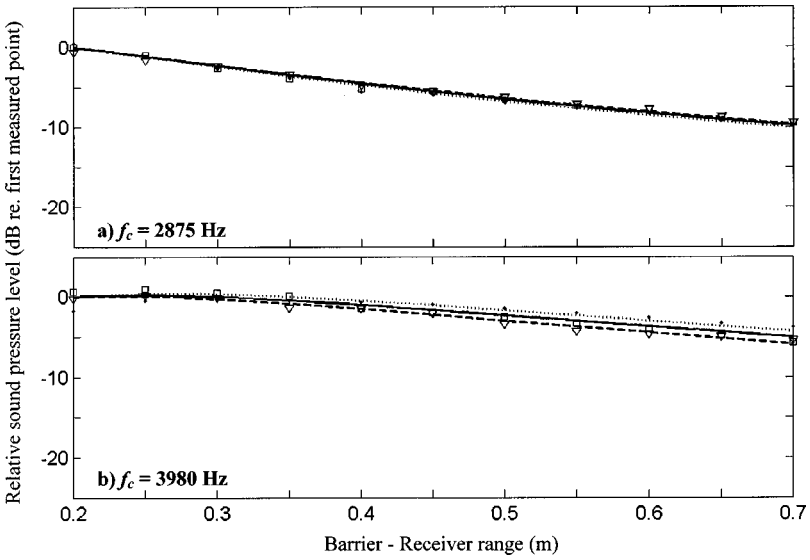

FIG. 17. The same as Fig. 15, except the ground is covered with carpet on both sides.

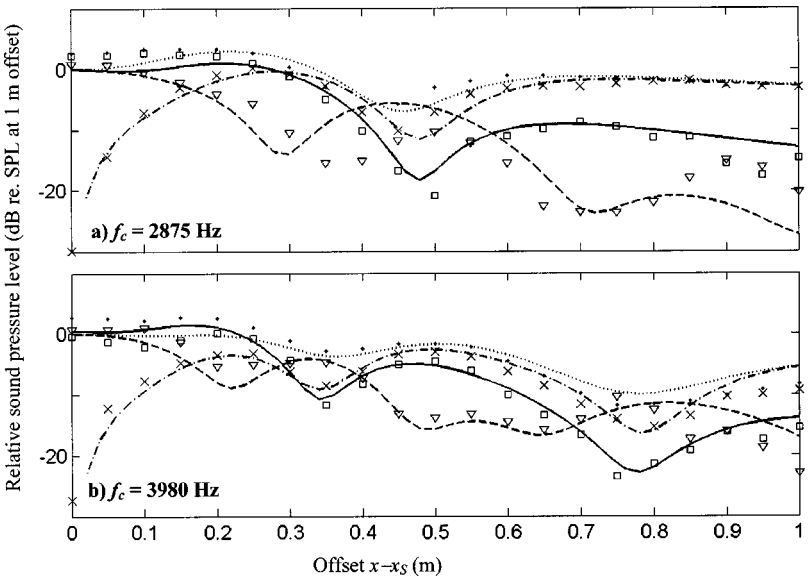

FIG. 18. Sound field as diffracted by a thin screen above hard ground as a function of the source–receiver offset $x-x_S$. Results are shown for a monopole source (dotted line: prediction; dots: measurements), a horizontal oriented along the y axis, perpendicularly to the edge of the screen (solid line: prediction; squares: measurements), a horizontal dipole oriented along the x axis, parallel to the edge (dashed–dotted line: prediction; crosses: measurements) and a vertical dipole (dashed line: prediction; triangles: measurements). The screen is 0.22 m high; both source and receiver are located at height 0.17 m; 0.1 away from the screen on each side. The results are referenced to the predicted SPL at null offset, except for the dipole along the x axis.

monopole for the ground reflection. On the other hand, its image with respect to the screen is inverted. It is the other way round for the vertical dipole whose sound field is similar to that due to a monopole as regards screen diffraction, but not for ground reflection. It appears from Figs. 15–17 that in the combination of both phenomena, the monopolar behavior is predominant. A remarkable consequence of this observation is in the acceptability of using monopole expressions as a rough estimate of the sound field due to directive sources in outdoor noise predictions involving barriers and screens for 2-D situations.

Finally, Fig. 18 shows the variations of the sound pressure level as a function of the source–receiver offset for our rigid thin screen above hard ground. Source and receiver are located relatively high above the ground: $z=z_S=0.17$ m—i.e., 0.05 m below the edge of the screen—and at a reasonably short distance away from the screen: $y=-y_S=0.1$ m. Four different sources were used: a monopole (dotted line: predictions; dots: measurements); a horizontal dipole along the y axis, perpendicular to the edge of the screen (solid line: predictions; squares: measurements); a horizontal dipole along the x axis, parallel to the edge (dashed–dotted line: predictions; crosses: measurements) and a vertical dipole (dashed line: predictions; triangles: measurements). Agreement between the experimental data and the predictions is generally very good. In view of the results shown in Fig. 18, the influence of the ground reflections is still critical, though the source and receiver are relatively high above the ground. This is confirmed by the fact that, unlike the vertical dipole and except when $kR \ll 1$, the horizontal dipoles behave in a way similar to a monopole source: with respect to the ground, the image source of a vertical dipole is inverted, whereas it keeps the original orientation in the case of a horizontal dipole. Unlike the 2-D situation, the dipole orientation seems to be crucial for the sound fields in the transverse direction when considering diffraction by a barrier in the presence of ground.

V. CONCLUDING REMARKS

A closed-form solution for the sound field due to a dipole source as diffracted by a hard wedge has been derived for arbitrary source and receiver positions. Based on Pierce's formulation for the diffraction of sound due to a point source,[2] this solution leads to an expression similar to the formulation according to Menounou's Directive Line Source Model.[6] By means of this solution for the diffracted dipole field, De Jong's semiempirical model for propagation above a ground discontinuity[4] has been extended. Similarly, an analytical formula has been derived for the calculation of the sound field due to dipole sources above the ground in the presence of a barrier. These practical cases have shown the influence of the source directivity on the prediction of the sound field. Particularly, in 2-D cases of barrier above ground, the dipole field is somewhat similar to that due to an omnidirectional point source. Nevertheless, in 3-D cases, the sound field in the transverse direction is very sensitive to the orientation of the source. This result is important in the context of screening of transportation noise where lines of incoherent dipoles may be used to model the noise source. For this reason, an extension of this work to more directional sources, such as quadrupoles, would be useful.

ACKNOWLEDGMENTS

The work reported in this paper has been conducted while one of the authors (M.B.) was on study leave at the Department of Mechanical Engineering, the Hong Kong Polytechnic University. The authors gratefully acknowledge the Research Committees of the Open University and the Hong Kong Polytechnic University for their partial financial support in this project. One of the authors (M.B.) was supported by an Open University Competitive Studentship. This work described in this paper was supported in part by EPRSC Grant No. GR L15326 and in part by the Research Grant Council of the Hong Kong SAR Government.

[1] J. J. Bowman and T. B. A. Senior, *Electromagnetic Waves and Acoustic Scattering by Simple Shapes* (North-Holland, Amsterdam, 1969).
[2] A. D. Pierce, "Diffraction of sound around corners and over barriers," J. Acoust. Soc. Am. **55**, 941–955 (1974).
[3] H. G. Jonasson, "Sound reduction by barriers on the ground," J. Sound Vib. **22**, 113–126 (1972).
[4] B. A. De Jong, A. Moekerken, and J. D. Van der Toorn, "Propagation of

sound over grassland and over an earth barrier,'' J. Sound Vib. **86**, 23–46 (1983).
[5] W. J. Hadden and A. D. Pierce, ''Sound diffraction around screens and wedges for arbitrary point source location,'' J. Acoust. Soc. Am. **69**, 1266–1290 (1981).
[6] P. Menounou, I. J. Busch-Vishniac, and D. T. Blackstock, ''Directive line source model: A new model for sound diffraction by half planes and wedges,'' J. Acoust. Soc. Am. **107**, 2973–2986 (2000).
[7] K. M. Li, M. Buret, and K. Attenborough, ''The propagation of sound due to a source moving at high speed in a refracting medium,'' *Proceedings of Euro-noise 98*, 1998, Vol. 2, pp. 955–960.
[8] A. D. Pierce, *Acoustics: An Introduction to its Physical Principles and Applications* (Acoustical Society of America, New York, 1989).
[9] P. M. Morse and U. Ingard, *Theoretical Acoustics* (McGraw-Hill, New York, 1968).
[10] K. M. Li, S. Taherzadeh, and K. Attenborough, ''Sound propagation from a dipole source near an impedance plane,'' J. Acoust. Soc. Am. **101**, 3343–3352 (1997).
[11] M. Abrahamowitz and I. Stegun, *Handbook of Mathematical Functions with Formulas, Graphs and Mathematical Tables*, 2nd ed. (Dover, New York, 1972).
[12] P. Boulanger, T. Watters-Fuller, K. Attenborough, and K. M. Li, ''Models and measurements of sound propagation from a point source over mixed impedance ground,'' J. Acoust. Soc. Am. **102**, 1432–1442 (1997).
[13] P. Koers, ''Diffraction by an absorbing barrier or by an impedance transition,'' *Proceedings of Internoise 83*, 1983, Vol. 1, pp. 311–314.
[14] K. Attenborough, ''Ground parameter information for propagation modeling,'' J. Acoust. Soc. Am. **92**, 418–427 (1997).
[15] D. D. Rife and J. Vanderkooy, ''Transfer-function measurements with Maximum Length Sequences,'' J. Audio Eng. Soc. **37**, 419–444 (1989).
[16] S. Peters, ''The prediction of Railway Noise Profiles,'' J. Sound Vib. **32**, 87–99 (1974).
[17] D. H. Cato, ''Prediction of environmental noise from fast electric trains,'' J. Sound Vib. **46**, 483–500 (1976).
[18] *Transportation Noise Reference Book*, edited by P. Nelson (Butterworths, London, 1987).